Observation of superconductivity and anomalous electrical resistivity in single-crystal Ir_{3}Te_{8}

L. Li, T. F. Qi, L. S. Lin, X. X. Wu, X. T. Zhang, K. Butrouna, V. S. Cao, Y. H. Zhang, Jiangping Hu, S. J. Yuan, P. Schlottmann, L. E. De Long, and G. Cao

Phys. Rev. B **87**, 174510 — Published 13 May 2013

DOI: 10.1103/PhysRevB.87.174510

Observation of Superconductivity and Anomalous Electrical Resistivity in Single-Crystal Ir_3Te_8

L. Li[1], T. F. Qi[1], L. S. Lin[2], X. X. Wu[3], X.T. Zhang[3], K. Butrouna[1], V. S. Cao[1#], Y. H. Zhang[2], Jiangping Hu[3,4], Shujuan Yuan[1,5], P. Schlottmann[6], L. E. De Long[1] and G. Cao[1*]

[1] Department of Physics and Astronomy and Center for Advanced Materials, University of Kentucky, Lexington, KY 40506, USA

[2] High Magnetic Field Laboratory, Chinese Academy of Sciences, Hefei 230031, China

[3] Beijing National Laboratory for Condensed Matter Physics, Institute of Physics, Chinese Academy of Sciences, Beijing, China

[4] Department of Physics, Purdue University, West Lafayette, IN 47907, USA

[5] Department of Physics, Shanghai University, Shanghai, China

[6] Department of Physics, Florida State University, Tallahassee, FL 32306, USA

Abstract

We observe an unusual combination of normal and superconducting state properties without any signature of strong spin fluctuations in single-crystal Ir_3Te_8. The electrical resistivity does not saturate by 700 K, but exhibits a low resistivity ratio; and it also exhibits two extended linear regimes (approximately 20 to 330 K and 370 to 700 K) with the same slope, separated by a small hysteretic interval marking a strongly first-order phase transition from cubic to rhombohedral lattice symmetry at T_S = 350 K. The electronic heat capacity coefficient (11 mJ/mole-K^2) is consistent with a net diamagnetic, rather than Pauli paramagnetic, normal state that yields to superconductivity below a critical temperature T_C = 1.8 K. The size of the heat capacity jump near T_C indicates bulk superconductivity.

I. Introduction

Ir compounds have recently emerged as a fertile ground for discoveries of new physics driven by large spin-orbit interactions (SOI) typical of 5d electronic states. The close competition between the SOI, crystalline electric fields, and the Coulomb interaction U stabilizes novel ground states and phenomena **[1-6]**. These discoveries have stimulated a variety of theoretical predictions **[7-13]** that await experimental confirmation, including topologically driven semimetallic **[12]** or superconducting **[13]** states.

Herein, we report an unusual combination of phenomena in single-crystal Ir_3Te_8: The normal state is metallic, but the electrical resistivity does not exhibit the usual T^2 Fermi liquid term. It does not saturate by 700 K and remains large (≈ 0.46 mΩ-cm) below 4 K. Moreover, Ir_3Te_8 is diamagnetic rather than Pauli paramagnetic [**21**], similar to non-superconducting Cu, since the core diamagnetism of Ir and Te ions is larger than the Pauli susceptibility. Ir_3Te_8 superconducts below a critical temperature T_C = 1.8 K, presumably due to a substantial electron-phonon coupling. It is remarkable that the resistivity slope remains essentially unchanged through a first-order phase transition at T_S = 350 K, which separates a high-temperature cubic phase from a low-temperature rhombohedral phase; this implies that the carrier density and the electron-phonon coupling is not affected by the structural change. Most structural and physical properties reported here are unique to single-crystal Ir_3Te_8 and have not been observed in polycrystalline samples **[20, 21]**.

Superconductivity has recently been found in Ir-based chalcogenides, namely CdI_2-type $Ir_{1-x}M_xTe_2$ (M = Pd and Pt) **[14-17]**, and Ir_xSe_2 (x > 0.75) pyrites **[18]**. Superconducting $Ir_{1-x}M_xTe_2$ is a derivative of layered $IrTe_2$, which exhibits a structural transition near 260 K from a rhombohedral, to a low-temperature,

monoclinic structure. This transition was attributed to a possible charge density wave (CDW) **[14]**, although no CDW gap has yet been detected **[16, 17]**. Nevertheless, superconducting transitions with T_C as high as 3 K emerge with the suppression of the structural transition in doped $Ir_{1-x}M_xTe_2$ **[14]**, similar to classic CDW compounds such as $NbSe_2$ and $(Nb_{1-x}Ta_x)Se_3$ **[18, 19]**. Higher T_C's of up to 6.4 K were found in a polycrystalline $Ir_{0.91}Se_2$ pyrite **[20]**, which is a nonstoichiometric variant of a parent $Ir_{0.75}Se_2$ (or Ir_3Se_8) compound of rhombohedral space group *R-3*, and is proximate to a metal-insulator transition. We note that no high-temperature phase transitions similar to that found in layered $IrTe_2$ are reported for relatively high-T_C Ir_xSe_2 compositions **[20]**. Superconductivity in these Ir-based chalcogenides is evidently not as sensitive to crystal structure as it is for many other transition metal materials, for which narrow peaks in the electronic density of states promote T_C's that range from 10 to 20 K **[22]**. Moreover, these chalcogenides sharply contrast with known Ir oxides, where a strong SOI generally drives narrow-gap insulating states **[1-2, 23-27]**.

II. Experimental

Single crystals of Ir_3Te_8 were grown by a slow-cooling technique using excess Te as flux. Stoichiometric quantities of the elements were ground thoroughly and sealed in an evacuated quartz tube, which was slowly heated up to 1000 ºC and held at that temperature for 7 days. The synthesized polycrystalline Ir_3Te_8 was then mixed with an appropriate amount of Te powder and sealed under vacuum in a small quartz tube, which was subsequently put in a larger quartz tube that was then evacuated and sealed. The mixture was heated up to 1050 ºC, where it was maintained for over 48 hours, followed by slow-cooling to 700 ºC. The average size of the single crystals was 1 x 1 x 1 mm^3, as shown in **Fig. 1**. Measurements of magnetization M(T,H), heat capacity C(T) and electrical resistivity ρ(T) were performed over the temperature

interval 0.5 K < T < 700 K, using either a Quantum Design (QD) Physical Property Measurement System, or a QD Magnetic Property Measurement System equipped with a Linear Research Model 700 AC bridge. The high temperature ρ(T) was measured using a Displex closed-cycle cryostat capable of continuous temperature ramping from 9 K to 900 K.

III. Band structure calculation

Density functional theory (DFT) calculations were carried out using the projector augmented wave (PAW) method encoded in the Vienna *ab initio* simulation package (VASP) **[28-30]**, and employed the generalized-gradient approximation (GGA) for the exchange correlation functional **[31]**. The SOI of the valence electrons was included using the second-variation method for the scalar-relativistic eigenfunctions of the valence states **[32]**. The plane-wave basis set cutoff was set at 500 eV. The Brillouin zone was sampled using the Monkhorst-Pack scheme **[33]** with (7×7×7) **k**-points for the Ir_3Te_8 and Ir_4Te_8 primitive cells. The lattice parameters used were a = 6.4024 Å and α = 90.017° (measured at 90 K; see **Table 1**). The atomic positions were fully relaxed and forces were minimized to less than 0.01 eV/Å.

IV. Results and Discussion

The crystal structure of a small single crystal was determined using Mo $K\alpha$ radiation and a Nonius Kappa CCD single-crystal diffractometer at temperatures T = 90 K, 250 K, 295 K, 350 K and 390 K. The structures were refined using the SHELX-97 programs **[34-35].** Crystal composition was examined by energy-dispersive X-ray (EDX) spectroscopy using a Hitachi/Oxford SwiftED 3000. The *R*- and R_W-factors are low, 0.025 and 0.058, respectively, and the mosaicity was also small, suggesting well-ordered crystals, as shown in **Figs. 1c** and **1d**. The Ir site occupancy was freely varied and found to be 80%. A superlattice was evident in all

X-ray diffraction data, suggesting that the Ir vacancies order in our crystals (see **Fig. 1b**). Given the possible existence of inhomogeneities in these materials **[15]**, the structural and physical properties of a number of Ir_3Te_8 crystals were examined, and we found no discernible discrepancies between data for all measured crystals. The 80% occupation of the Ir sites gives rise to disorder scattering of the conduction electrons and is a likely explanation for the large residual resistivity.

The room-temperature crystal structure of Ir_3Te_8 was initially reported to be cubic with space group *Pa3* **[36]**, but was subsequently described as rhombohedral with space group *R-3* **[37]**. Our single-crystal X-ray refinements show Ir_3Te_8 undergoes a structural phase transition near T_S = 350 K, changing from a high-temperature cubic lattice with space group *Pa3* (No. 205) to a low-temperature rhombohedral lattice with space group *R-3* (No. 148) (see **Table 1**). The difference between the two structures can be defined by the difference $\Delta\theta$ ($\equiv \theta_1-\theta_2$) between two bond angles θ_1 (Ir1-Te1-Ir2) and θ_2 (Ir2-Te2-Ir1); i.e., $\Delta\theta$ is zero for $T \geq T_S$ = 350 K when the lattice is cubic, and finite for $T < T_S$ where the lattice symmetry is reduced to rhombohedral (see **Figs. 1a** and **1b**). The structural transition is subtle, but nevertheless causes strong anomalies in the transport and magnetic properties, as discussed below.

Table 1: ***Lattice Parameters for Ir_3Te_8***

Temperature (K)	**90**	**250**	**390**
***a* (Å)**	6.4024	6.4081	6.4152
α(°)	90.017	90.017	90
Structure (Space group)	Rhombohedral (*R-3*)	Rhombohedral (*R-3*)	Cubic (*Pa3*)

Our heat capacity data C(T) for 50 mK ≤ T < 300 K yield a Debye temperature θ_D = 246 K, and an electronic coefficient $\gamma = 11$ mJ/mole K^2. These values are quite similar to those for Ir_xSe_2 **[20]**. Single-crystal Ir_3Te_8 is distinctly metallic (although highly resistive) throughout a wide temperature range (see **Fig. 2a**), which sharply contrasts the insulating behavior of Ir_3Se_8 **[20]**. The **a**-axis electrical resistivity $\rho_a(T)$ is interrupted by a strong first-order anomaly with hysteresis in the vicinity of T_S = 350 K, which is consistent with the lattice transition revealed in the structural data. Except for T < 20 K (including an onset of superconductivity at T_C = 1.8 K) and the vicinity of T_S, the slope of $\rho_a(T)$ remains unchanged over a remarkably wide temperature range, 20 K ≤ T ≤ 700 K, in particular, both below and above T_S.

An extended regime of linear-T resistivity is a classic signature of high-T_C cuprates and the p-wave superconductor Sr_2RuO_4, Fe-based superconductors and many other correlated oxides **[38]**, in which spin fluctuations play an important role in the electron scattering. In contrast, Ir_3Te_8 is diamagnetic (see below), and the application of high magnetic fields up to 14 T causes no changes near the anomaly at T_S, or $\rho_a(T)$ at $T >> T_C$ (not shown). These observations confirm that the observed behavior in $\rho_a(T)$ for Ir_3Te_8 must have an origin other than spin scattering. Elementary Bloch-Grüneisen theory predicts $\rho(T) \sim T^5$ for $T < (0.2)\ \theta_D \sim 49$ K (we find the Debye temperature θ_D = 246 K for Ir_3Te_8), and $\rho(T) \sim T$ for $T >> \theta_D$, in the case of electron-phonon scattering. The linearity of resistivity in an extended regime is seen for some elements, such as copper and platinum. However, only a handful of materials exhibit an extended regime of linear-T resistivity that accompanies superconductivity; indeed, "resistivity saturation" is anticipated when the mean-free path *l* of the quasiparticles becomes shorter than the lattice parameter *a* (Mott-Ioffe-Regel limit **[39, 40]**), or for $\rho \sim$ 100-150 μΩ cm (Mooij limit, **[41, 42]**). The

experimental values of $\rho_a(T)$ for Ir_3Te_8 are well above the Mott-Ioffe-Regel or Mooij limits, yet $\rho_a(T)$ shows no sign of saturation up to 700 K. What is intriguing is that $\rho_a(T)$ shows no slope change near T_S, despite the fact that the first-order structural change that must affect the electronic state. At low temperatures, $\rho_a(T)$ shows a Kondo-like minimum near 20 K without the usual T^2 Fermi liquid term, but it remains large (the residual resistivity $\rho_o \approx 0.46$ mΩ-cm) between T_C and 10 K (**Fig. 2a**). It deserves to be pointed out that, in spite of the large residual resistivity, the overall change in $\rho_a(T)$ between 10 and 700 K or $\rho_a(T) - \rho_o$ is of order 180 μΩ-cm (see the **Fig. 2a inset**), which is quite reasonable for a low-density-of-states material ($\gamma = 11$ mJ/mol Ir-K^2), and consistent with both T_C and our specific heat jump data discussed below. This also shows that the overall change of resistivity is sufficient to clearly define a temperature power law of the high-temperature resistivity.

The magnetic susceptibility $\chi(T)$ of Ir_3Te_8 up to room temperature has been reported previously **[21]**. The susceptibility for single crystals is anisotropic; remarkably, $\chi_{[111]}$ is more diamagnetic than χ_a, and both exhibit a first-order anomaly in the vicinity of T_S, as shown in **Fig. 2b**. An unusually strong thermal hysteresis is seen in **Fig. 2b**, consistent with a structural transition. Both $\chi_{[111]}(T)$ and $\chi_a(T)$ rapidly rise below 30 K; a Curie-Weiss fit of $\chi_{[111]}$ (warming portion) for $T < 30$ K yields a Curie-Weiss temperature $\theta_{CW} = -0.7$ K and a small effective moment $\mu_{eff} = 0.024\ \mu_B$/Ir. Both the low-temperature susceptibility and the minimum in $\rho_a(T)$ near 12 K suggest a small concentration of impurity spins is present (see the **Inset** in **Fig. 2b**). Note that these impurity spins could be Ir-ions with incomplete bonding. The net diamagnetic moment may not be entirely surprising, given the small value of the Sommerfeld heat capacity coefficient $\gamma \approx 11$ mJ/mole-K^2, i.e. per three Ir ions, which

is only slightly larger and comparable to that for diamagnetic Cu. The diamagnetism is due to the fact that both Ir and Te are heavy elements, and they have large core diamagnetism (χ_d(Te) = -7 x 10^{-5} emu/mole and χ_d(Ir) = -3.5 x 10^{-5} emu/mole **[37]**) that exceeds the Pauli paramagnetism. The net core diamagnetism is estimated to be -6.7 x 10^{-4} emu/mole-Ir_3Te_8, which is consistent with the experimental value of -3.5 x 10^{-4} emu/mole, considering that there must be a compensating contribution from the Pauli paramagnetism. It is noted that this scenario offers no clear explanation for the significant anisotropy of χ(T) illustrated in **Fig. 2b**, which has to arise from the paramagnetic term, e.g. due to Van Vleck band contributions that reflect anisotropies of the electronic structure and/or small gaps between bands near the Fermi level (see below).

The transition of Ir_3Te_8 to superconductivity is shown in **Fig. 3**, where both ρ_a(T) and χ_a(T) exhibit onsets at T_C = 1.8 K. ρ_a(T) drops by one order of magnitude from T_C=1.80 K to 1.2 K, but does not vanish at 1.2 K (ρ_a(1.2K) = 4.5 x 10^{-5} Ω cm). The relatively broad transition is unusual but consistent with the jump in the specific heat C(T) and the weak short-range magnetic order evidenced in the data shown in **Figs.2** and **3**. Indeed, application of a DC magnetic field H readily depresses T_C (see **Fig. 3a inset**), as expected. On the other hand, ρ_a(T) exhibits a small positive magnetoresistive shift for T > T_C. If this would be due to short-range antiferromagnetic order or a Kondo-like effect one would anticipate a negative magnetoresistance. Note that χ_a(T) exhibits little difference between zero-field-cooling (ZFC) and field-cooling (FC) measurements until the temperature decreases to 0.5 K, as illustrated in **Fig. 3b**. This indicates the superconducting state may not be fully established until well below 0.5 K. Nevertheless, an "equal-area" (entropy balancing) construction of the heat capacity data near T_C (see **Fig. 4**) yields a

conservative estimate of $\Delta C/\gamma T_C \approx 1.0$, which indicates bulk superconductivity; this estimate is also consistent with the partial suppression of the superconducting gap (corresponding to the fully gapped value $\Delta C/\gamma T_C \approx 1.43$ for the BCS model with $\gamma \approx$ 11 mJ/mole fu-K^2) by pairbreaking due to magnetic impurities **[43]**. These scenarios are also consistent with estimates of an approximate 16% Meissner effect at 0.5 K, when the demagnetization effect and flux pinning are taken into account. We conclude that a sizable superconducting volume exists in our crystal, even if the superconducting state is incompletely established over a substantial range of temperature near T_C.

Our electronic structure calculations for Ir_3Te_8 were performed by first carrying out a calculation for Ir_4Te_8, then removing the Ir atoms located at the Wyckoff site *a* in a unit cell. Two bands derived from Ir-e_g and Te-*5p* orbitals cross the Fermi level E_F in the case of Ir_3Te_8, as shown in **Fig. 5**. The band structure of Ir_3Te_8 contrasts that of Ir_3Se_8, where only one band crosses E_F **[20]**. The calculations with or without the SOI do not seem to yield a noticeable difference in the band structure, chiefly because the states near E_F consist of Ir-e_g or d_z^2 orbitals rather than Ir-t_{2g} orbitals (for which the SOI is a first-order effect).

At $T > T_S = 350$ K, the electronic structure near the Fermi surface is formed primarily by **(1)** the σ* anti-bonding bonding state of two Te atoms at the center of the cubic unit cell, and **(2)** one symmetrized state formed from the d_z^2 orbitals of the three Ir atoms at positions (1/2,1/2,0), (0,1/2,1/2) and (1/2,0,1/2), which results in a band having strong energy dispersion along the [111] direction. At $T < T_S$, the rhombohedral phase is characterized by two distinct Wyckoff positions *a* and *e* in space group *R-3*; the d_z^2 orbitals of the three Ir ions at the position *e* form a band with some quasi-two-dimensional characteristics. Following a general Landau-Ginzburg

symmetry argument, any perturbation of the electronic structure (e.g., via even a weak electron-phonon coupling) in Ir_3Te_8 must lead to a lattice symmetry breaking, which explains the structural transition at T_S = 350 K. When an external magnetic field is applied along the [111] direction, a diamagnetic current loop is induced to flow between the three Ir atoms coupled via the symmetrized state of the d_z^2 orbitals. Moreover, the expected diamagnetism must be anisotropic, and the diamagnetic response along [111] should be stronger than that along other directions, which is also consistent with the data shown in **Fig. 2b**. This could be an alternative explanation for the anisotropic diamagnetism.

There is an important difference between Ir-telluride and the iridates. The oxygen atoms in the iridates carry two additional electrons to complete their *p*-shell. The crystalline field splitting of the Ir ions is then essentially given by a point charge model. In sixfold coordination this yields the t_{2g}-orbitals below the e_g-states. The t_{2g}-orbitals have substantial spin-orbit coupling (e.g. in first order perturbation) and hence the physics of the iridates is spin-orbit driven. On the other hand, the Te-orbitals participate in covalent bonding. The bonds are directed in the *x*, *y* and *z* directions of the octahedra. Hence, the energy of the Ir e_g-orbitals is lowered more than the energy of the t_{2g}-states. Hence, the crystalline electric field scheme is reverted with respect to the iridates. The e_g-orbitals are much less susceptible to the SOI than the t_{2g}-states and hence Ir_3Te_8 is not driven by the SOI.

V. Summary

All results of Ir_3Te_8 presented here indicate an occurrence of bulk superconductivity below T_C = 1.8 K; the superconductivity is accompanied by diamagnetism and unsaturated resistivity that persist over an unusually wide temperature interval 20 K < T < 700 K spanning a structural transition at T_S = 350 K,

through which the resistivity slope remains unchanged. The observed lattice transition could be attributed to quasi-two-dimensional properties of a band crossing at the Fermi level. However, the relationship of the superconducting state below T_C = 1.8 K to the structural phase transition, the unusual normal state, and the incomplete occupation of the Ir sites in Ir_3Te_8 pose a challenge to our understanding of Ir-based materials.

This work was supported by NSF through grants DMR-0856234 and EPS-0814194; JPH acknowledges support by the Ministry of Science and Technology of China 973 program (2012CB821400) and NSFC-1190024. LED and PS acknowledge the support of U.S. Dept. of Energy Grants No. DE-FG02-97ER45653 and DE-FG02-98ER45707, respectively. XXW thanks H. M. Weng for enlightening discussions. We thank Dr. Neil Dilley at the Quantum Design for measurements of mK heat capacity and electric resistivity.

High school student, Paul Lawrence Dunbar High School, Lexington, KY 40513

* Corresponding author; email: cao@uky.edu

References

1. B. J. Kim, Hosub Jin, S. J. Moon, J.-Y. Kim, B.-G. Park, C. S. Leem, Jaejun Yu, T. W. Noh, C. Kim, S.-J. Oh, V. Durairai, G. Cao, and J.-H. Park*, Phys. Rev. Lett*. **101**, 076402 (2008).
2. S.J. Moon, H. Jin, K.W. Kim, W.S. Choi, Y.S. Lee, J. Yu, G. Cao, A. Sumi, H. Funakubo, C. Bernhard, and T.W. Noh, *Phys. Rev. Lett*. **101**, 226401 (2008).
3. B.J. Kim, H. Ohsumi, T. Komesu, S.Sakai, T. Morita, H. Takagi, T. Arima, *Science* **323**, 1329 (2009).
4. L. Fu, C. L. Kane, and E. J. Mele, *Phys. Rev. Lett*. **98**, 106803 (2007).
5. J. E. Moore and L. Balents, *Phys. Rev. B* **75**, 121306(R) (2007).
6. Y. Xia, D. Qian, D. Hsieh, L. Wray, A. Pal, H. Lin, A. Bansil, D. Grauer, Y. S. Hor, R. J. Cava & M. Z. Hasan, *Nature Physics* **5**, 398 (2009).
7. Fa Wang and T. Senthil, *Phys. Rev. Lett.* **106**, 136402 (2011).
8. Xiangang Wan, A. Vishwanath, S.Y. Savrasov, *Phys. Rev. Lett*. **108**, 146601 (2012)
9. B.J. Yang and Y.B. Kim, *Phys. Rev. B* **82**, 085111 (2010).
10. Atsuo Shitade, Hosho Katsura, Jan Kuneš, Xiao-Liang Qi, Shou-Cheng Zhang and Naoto Nagaosa, *Phys. Rev. Lett.* **102**, 256403 (2009).
11. D.A. Pesin, and Leon Balents, *Nat. Phys*. **6**, 376 (2010).
12. Yi Zhou, Patrick A. Lee, Tai-Kai Ng and Fu-Chun Zhang, *Phys. Rev. Lett.* **101**, 197201 (2008).
13. L. Fu and E. Berg, *Phys. Rev. Lett.* **105**, 097001 (2010).

14. J. J. Yang, Y. J. Choi, Y. S. Oh, A. Hogan, Y. Horibe, K. Kim, B. I. Min, and S-E. Cheong. *Phys. Rev. Lett.* **108**, 116402 (2012).

15. S.Y. Zhou, B.Y. Pan, X. Qiu, J. Pan, X. C. Hong, X. L. Li, Z. Zhang, J. J. Yang, Y. S. Oh, S-W. Cheong, and S. Y. Li, arXive:1209.4229, 2012.

16. A. F. Fang, G. Xu, T. Dong, P. Zheng, and N. L. Wang, arXiv:1203.4061, 2012.

17. D. Ootsuki, S. Pyon, K. Kido, M. Nohara, M. Horio, T. Yoshida, A. Fujimori, M. Arita, H, Anzai, H. Namatame, M. Taniguchi, N. L. Saini, and T. Mizokawa, arXive: 1207. 2613. 2012.

18. T. F. Smith, L. E. De Long, A. R. Moodenbaugh, T. H. Geballe and R. E. Schwall, *J. Phys. C: Solid State Phys.* **5**, L230-L232 (1972).

19. K. Kawabata, *J. Phys. Soc. Japan* **54**, 762-770 (1984).

20. Yangpen Qi, Storu Matsuishi, Jiangang Guo, Hiroshi Mizoguchi and Hideo Hosono, *Phys. Rev. Lett*. **109**, 217002 (2012).

21. P.C. Liao, C.H. Ho, Y.S. Huang, K.K. Tiong, J. Crystal Growth **171**, 586 (1997).

22. E. A. Lynton, *Superconductivity* (Methuen, London, 1969), Chapt. 1.

23. G. Cao, J. Bolivar, S. McCall, J.E. Crow, and R.P. Guertin, *Phys. Rev. B* **57**, **R** 11039 (1998).

24. G. Cao, J.E. Crow, R.P. Guertin, P. Henning, C.C. Homes, M. Strongin, D.N. Basov, and E. Lochner, *Solid State Comm.* **113**, 657 (2000).

25. G. Cao, Y. Xin, C. S. Alexander, J.E. Crow and P. Schlottmann, *Phys. Rev. B* **66**, 214412 (2002).

26. O. B. Korneta, S. Chikara, L.E. DeLong. P. Schlottmann and G. Cao, *Phys. Rev. B* **81**, 045101 (2010).

27. M. Ge, T. F. Qi, O.B. Korneta, L.E. De Long, P. Schlottmann and G. Cao, *Phys. Rev. B* **84**, 100402(R) (2011).

28. G. Kresse and J. Hafner, *Phys. Rev. B* **47**, 558 (1993).

29. G. Kresse and J. Furthmuller, *Comput. Mater. Sci.* **6**, 15 (1996).

30. G. Kresse and J. Furthmuller, *Phys. Rev. B* **54**, 11169 (1996).

31. J. P. Perdew, K. Burke, and M. Ernzerhof, *Phys. Rev. Lett.* **77**, 3865 (1996).

32. D. D. Koelling and B. N. Harmon, *J. Phys. C* **10**, 3107 (1977).

33. H. J. Monkhorst and J. Pack, *Phys. Rev. B* **13**, 5188 (1976).

34. G. M. Sheldrick, *Acta Crystallogr.* A **64**, 112 (2008).

35. G. M. Sheldrick, *SADABS* (University of Göttingen, Germany), 1996.

36. E. F. Hocking and J. G. White, *J. Phys. Chem.* **64**, 1042 (1960).

37. S. Jobic, M. Evain, R. Brec, P. Debiard, A. Jouanneaux and J. Rouxel, J. *Solid State Chem.* **95**, 319 (1991).

38. G. Cao, W.H. Song, Y.P. Sun and X.N. Lin, *Solid State Comm.* **131**, 331 (2004).

39. N.F. Mott, *Philos. Mag*. **26**, 1015 (1972).

40. A.F. Ioffe and A.R. Regel, *Prog. Semicond.* **4**, 237 (1960).

41. J.H. Mooij, *Phys. Status Solidi* A **17**, 521 (1973).

42. M. Weger and N.F. Mott, *J. Phys. C: Solid St. Phys*. **18**, L201 (1985).

43. M. B. Maple and Kang-Soo Kim, *Phys. Rev. Lett*. **23**, 118 (1969).

Captions

Fig.1. **(a)** The crystal structure of Ir_3Te_8; **(b)** the definition of the bond angles, θ_1 and θ_2 (upper panel) and the temperature dependence of θ_1 and θ_2 (lower panel); **(c)** a representative x-ray diffraction pattern at T=295 K for [*h* 1 *l*]; and **(d)** representative single crystals of Ir_3Te_8.

Fig. 2. **(a)** The temperature dependence of the a-axis resistivity $\rho_a(T)$ for 1.7 K $\leq$ T $\leq$ 700 K. **Inset**: $(\rho_a(T)- \rho_o)$ as a function of temperature for 10 K $\leq$ T $\leq$ 700 K. **(b)** The temperature dependence of the magnetic susceptibility $\chi_{[111]}(T)$ along the direction [111] and $\chi_a(T)$ along the a-axis at μ_oH = 0.5 T for 1.7 K $\leq$ T $\leq$ 395 K. **Inset**: $(\Delta\chi)^{-1}_{[111]}$ vs. T for 1.7 K $\leq$ T $\leq$ 30 K, where $\Delta\chi_{[111]} \equiv \chi_{[111]} - \chi_o$, and χ_o= -0.000372 emu/mole).

Fig. 3. The temperature dependence of **(a)** the a-axis resistivity $\rho_a(T)$ for 1.0 K $\leq$ T $\leq$ 10 K; and **(b)** the a-axis magnetic susceptibility $\chi_a(T)$ for 0.5 K $\leq$ T $\leq$ 10 K at μ_oH = 0.005 T. **Inset:** The temperature dependence of $\rho_a(T)$ for 1.7 K $\leq$ T $\leq$ 10 K at μ_oH = 0, 0.5, 1, and 5 T.

Fig. 4. The specific heat C(T) divided by temperature C(T)/T as a function of T^2 for 50 mK $\leq$ T $\leq$ 10 K.

Fig. 5. The band structures and density of states (DOS) of **(a)** Ir_4Te_8 and **(b)** Ir_3Te_8; and **(c)** Fermi surfaces for Ir_3Te_8: the lower band (left) and the higher band (right). Γ is the center of the Brillouin Zone, R (0.5, 0.5, 0.5), X (0, 0.5, 0) and M (0.5, 0.5, 0). The total DOS and momentum projected-DOS are shown in the middle panel and right panel in **(a)** and **(b)**, respectively. The middle letters are the Wyckoff positions; for instance, "Ir-e-5d" represents the 5d orbital projected-DOS of Ir at positions *e*.

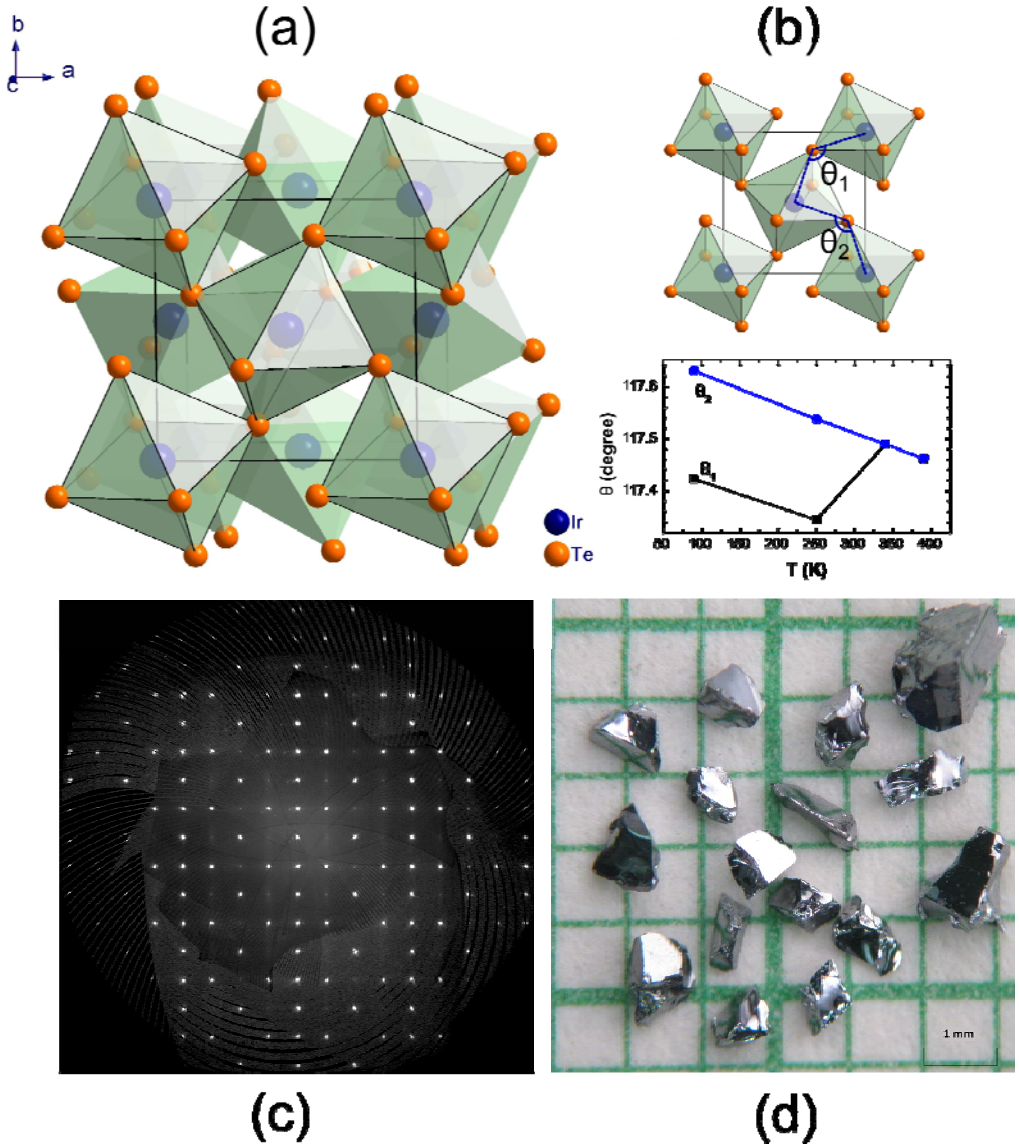
(a)
b
a
c
Ir
Te
(b)
θ1
θ2
θ2
θ1
117.6
117.5
117.4
θ (degree)
60
100
150
200
250
300
350
400
T (K)
(c)
(d)
1 mm

Fig.1

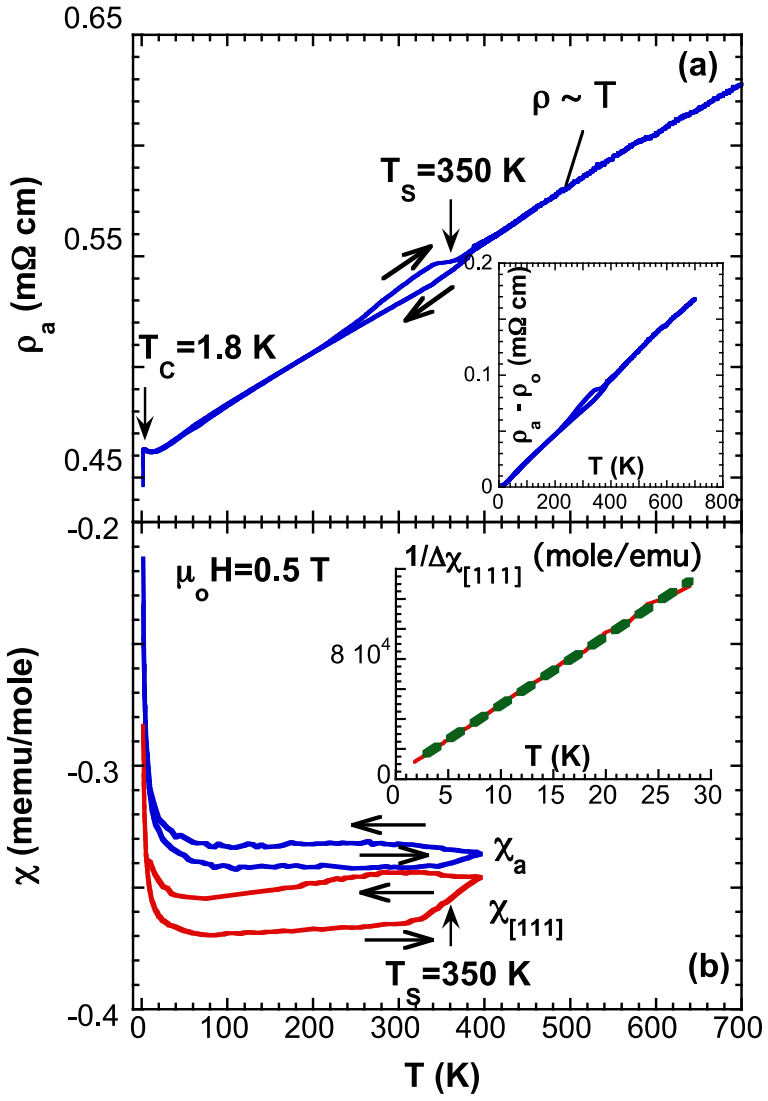
(a)
ρ ~ T
T_s=350 K
T_c=1.8 K
ρ_a (mΩ cm)
ρ_a - ρ_o (mΩ cm)
T (K)
μ_o H=0.5 T
1/Δχ_[111] (mole/emu)
8 10^4
χ (memu/mole)
χ_a
χ_[111]
T_s=350 K
(b)
T (K)

Fig. 2

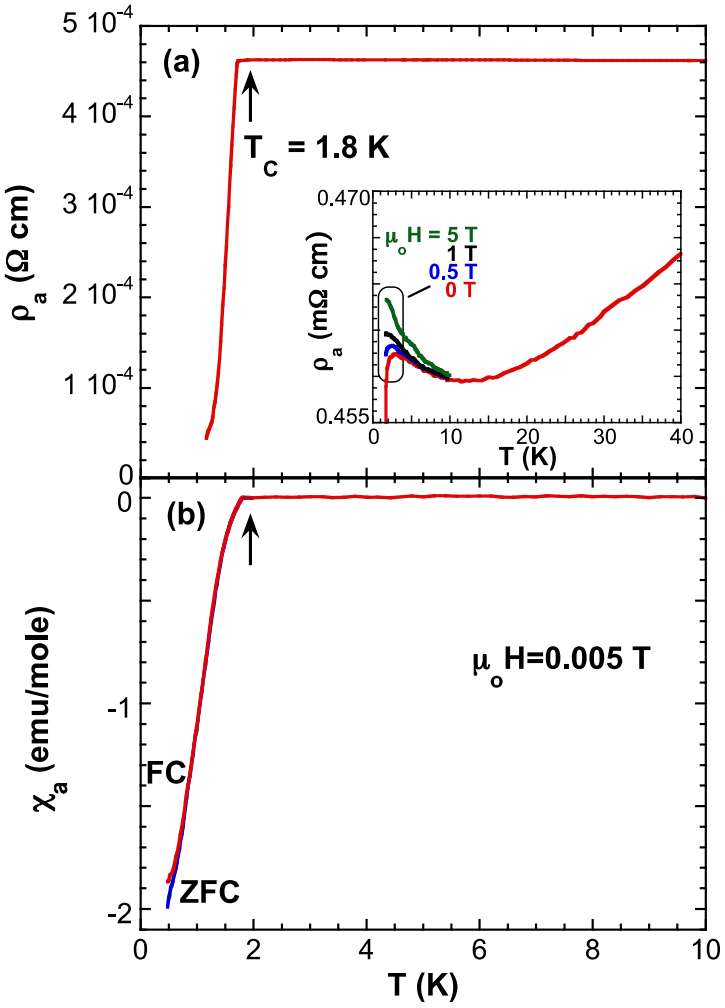
(a)
T_c = 1.8 K
ρ_a (Ω cm)
5 10^{-4}
4 10^{-4}
3 10^{-4}
2 10^{-4}
1 10^{-4}
0
ρ_a (mΩ cm)
0.470
0.455
μ_oH = 5 T
1 T
0.5 T
0 T
0
10
20
30
40
T (K)
(b)
χ_a (emu/mole)
μ_oH=0.005 T
FC
ZFC
0
-1
-2
0
2
4
6
8
10
T (K)

Fig. 3

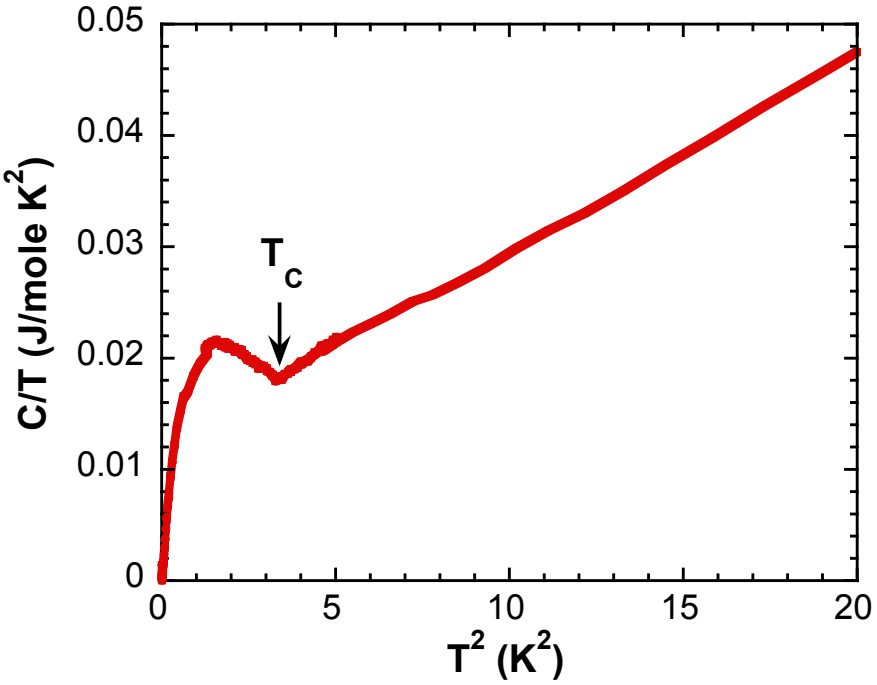

Fig. 4

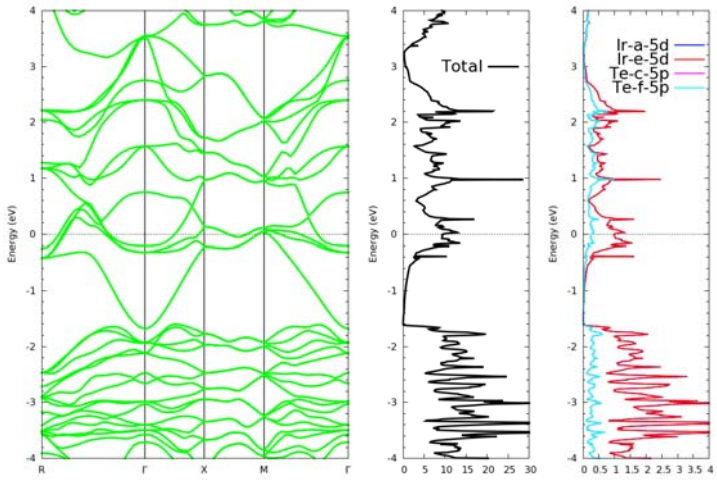
Energy (eV)
R
Γ
X
M
Γ
Total
Ir-a-5d
Ir-e-5d
Te-c-5p
Te-f-5p

(a)

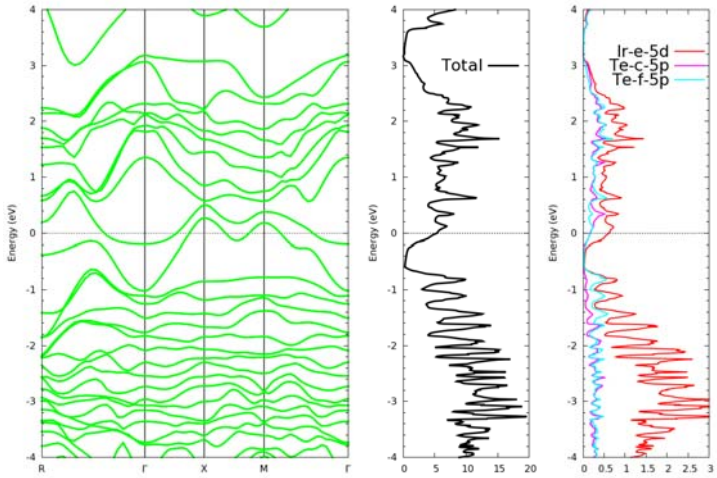
Energy (eV)
R
Γ
X
M
Γ
Total
Ir-e-5d
Te-c-5p
Te-f-5p

(b)

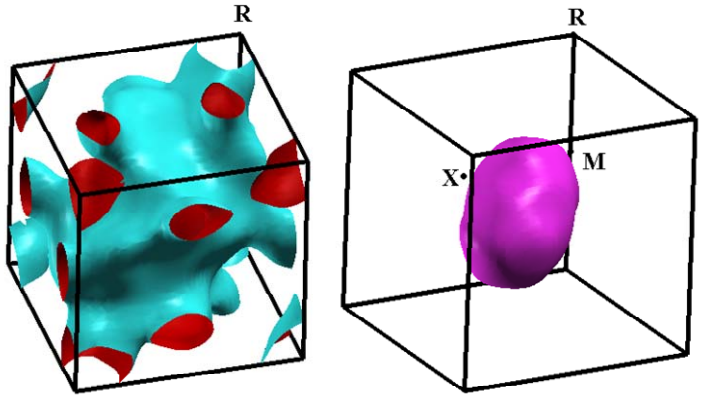
R
R
X
M

(c) **Fig. 5**